The melting curve of MgO from first principles simulations

Dario Alfè

Department of Earth Sciences, and Department of Physics and Astronomy,
University College London, Gower Street, London, WC1E 6BT, U.K

First principles calculations based on density functional theory, both with the local density approximation (LDA) and with generalised gradient corrections (GGA), and the projector augmented wave method, have been used to simulate solid and liquid MgO in direct coexistence in the range of pressure $0 \leq p \leq 135$ GPa. The calculated LDA zero pressure melting temperature is $T_m^{\mathrm{LDA}} = 3110 \pm 50$ K, in good agreement with the experimental data. The calculated GGA zero pressure melting temperature $T_m^{\mathrm{GGA}} = 2575 \pm 100$ K is significantly lower than the LDA one, but the difference between the GGA and the LDA melting curves is greatly reduced at high pressure. The LDA calculated zero pressure melting slope is $dT/dp \sim 100$ K/GPa, which is more than three times higher than the currently available experimental one ((Zerr and Boehler, Nature **371**, 506 (1994)). As the pressure is increased, the melting curve deviates significantly from the experimental one. At the core mantle boundary pressure of 135 GPa MgO melts at $T_m = 8140 \pm 150$ K.

MgO (periclase) is a very important material for a number of reasons. At ambient conditions it has the rock-salt structure of NaCl, and has the peculiarity of not showing any phase transition at least up to 227 GPa [1]. For this reason it is often used as a pressure medium in high pressure solid media devices. The periclase related structure Mg(Fe)O-magnesiowüstite is believed to be present in large quantities in the Earth's lower mantle, therefore knowledge of the behaviour of MgO under pressure is very important for our understanding of the lower mantle. In particular, the melting behaviour of periclase under pressure is important to put constraints on the solidus in the lower mantle: a low melting temperature of periclase may point to a low eutectic point, and in particular may support the suggestions of the presence of partial melt in the 'ultra-low velocity zone' [2].

The only available experiment for the melting behaviour of MgO under pressure has been performed by Zerr and Boehler [3] (ZB), who measured the melting curve of MgO up to 32 GPa. They found a slope of the melting curve at zero pressure $dT_m/dp \sim 30$ K/GPa, and a relatively low extrapolated melting temperature at lower mantle pressures; a result which may support the presence of partial melt at the bottom of the mantle.

A number of theoretical calculations, based on empirical potentials, have attempted to determine the melting curve of periclase up to lower mantle pressures [4–8]. The results of these calculations are somewhat scattered, but they all predict significantly higher than experiments zero pressure melting slopes, and consequently much higher melting temperatures of periclase at lower mantle pressures.

Here I report first principles calculations of the whole melting curve of MgO in the pressure range 0-135 GPa. Melting points have been calculated by performing direct first principles simulations of solid and liquid MgO in coexistence. Since a large number of atoms is needed to represent correctly solid and liquid in equilibrium,

the method is extremely computationally intensive, however, the feasibility of the coexistence approach within first principles calculations has been recently demonstrated [9–11]. In the constant volume constant internal energy (NVE ensemble) approach to the coexistence method it has been shown that liquid and solid can coexist for long times, provided V and E are appropriately chosen [9,12,13]. The average value of the pressure p and temperature T over the coexisting period then give a point on the melting curve. Size effects have been studied quite extensively, and it was shown that correct results, including in MgO, can be obtained in systems containing more than 500 atoms [6,9,14,15], although recent calculations on LiH have also been performed on system containing 432 atoms [10].

The zero pressure crystal structure of MgO is the same as the NaCl structure, and since no transitions have been experimentally observed up to at least 227 Gpa [1], I assumed that melting occurs from this structure. However, I note that at high temperature this is not necessarily true, and melting may occour from a different crystal structure, as recently suggested by Aguado and Madden [16]. The existence of a more stable solid phase would increase the melting temperature.

A possible source of error in the calculations may be due to the neglecting of the formation of defects in the solid. Although defects formation is not explicitly excluded in the current approach, it is unlikely that the simulations are long enough to allow for significant ionic diffusion in the solid. A concentration c of defects would be responsible for a decrease of the solid Gibbs free energy per atom $g_{\mathrm{v}} \sim -k_{\mathrm{B}}Tc$ [17], and a consequent increase in the melting temperature $\delta T_m \sim g_{\mathrm{v}}/s_m$, where s_m is the entropy of melting. The concentration c of defects in MgO near the melting temperature is given by $c = \exp\{-E_{\mathrm{v}}/2k_{\mathrm{B}}T\}$, where E_{v} is the formation energy of the defect. An estimate of c comes from the value of the formation energy of a Schottky defect, which in

MgO has a value between 4 and 7 eV [18]. Recent density functional theory (DFT) [19,20] and quantum Monte Carlo [20] calculations point to a value close to 7 eV, but even using the lower value 4 eV, and $T = 3000$ K for the melting temperature, we obtain $c \sim 6 \times 10^{-4}$, which results in a completely negligible correction to the melting temperature.

Present calculations have been performed using density functional theory with various approximations for the exchange-correlation (XC) functional. I used the VASP code [21], with the implementation of an efficient extrapolation of the charge density [22], and the projector augmented wave (PAW) method [23,24]. Single particle orbitals have been expanded in plane-waves, with a plane-wave cutoff of 400 eV. The Mg potential has a core radius of 1.06 Å, and the $3s^2$ electrons in valence; the O potential has a core radius of 0.8 Å and the $2s^2 2p^4$ electrons in valence. The structural properties of MgO in its rock-salt zero pressure crystal structure are compared with the experimental results in Table I. Pressure against volume curves are compared with experiments in the inset of Fig. 1. In Table I I also report the value of the transition pressure between the rock-salt and the CsCl structures, which is in the region of 500 GPa. I also tested a "small core" Mg potential with both $3s^2$ and $2p^6$ electrons in valence. Results are reported in Table I. The zero temperature MgO crystal has a band gap of several eV's, but this gap is significantly reduced at high temperature, where electron excitations become important, therefore finite temperature calculations have been performed by minimising the Mermin functional [25]. In fact, the electronic entropy contribution to the free energy of the system is non-negligible, and at zero pressure it lowers the free energy of the liquid with respect to the free energy of the solid by almost 0.1 eV. Given a zero pressure entropy of melting is ~ 2.2 k_B/atom (see Tab II), the electronic entropy is responsible for a lowering of the zero pressure melting temperature of ~ 500 K.

The coexistence simulations have been performed using the local density approximation (LDA) for the XC functional, and the Mg potential with only $2s^2$ in valence, using the NVE ensemble for systems containing 432 atoms ($3 \times 3 \times 6$ cubic supercell). The time step was 1 fs and the convergency threshold on the total energy 2×10^{-8} eV/atom. With these prescriptions the drift in the micro-canonical total energy was less than 0.5 K/ps. Simulations were carried out for up to 20 ps, and performed using the Γ point only. Spot checks with Monkhorst-Pack [26] ($2 \times 2 \times 1$) and ($2 \times 2 \times 2$) **k**-point grids showed energies converged better than 0.1 meV/atom and pressure converged better than 1 MPa. A correction term of 3.7 (5.7) GPa due to the lack of convergency with respect to the plane wave cutoff has been added to the calculated pressures in the low (high) pressure regions.

To prepare the system I have followed the same procedure employed in Refs. [9,13]. A perfect crystal is initially thermalized to a guessed melting temperature T_{guess}, then the simulation is stopped, half of the atoms are clamped and the other half are freely evolved at very high temperature until melting occurs, then the liquid is thermalized back at T_{guess}. At this point the system is being freely evolved in the NVE ensemble. Note that in (V, E) space melting is represented by a "band", and not by a line as in (p, T) space. In particular, for every fixed V, a whole piece of melting curve can be evaluated by varying E appropriately. The amount of total energy E given to the system can be tuned by assigning different initial values to the velocities [27]. Now, unless the value of E is in the right range for the volume V, the system will either completely melt or completely solidify. For MgO this happens very quickly, typically in less than 1 ps. Therefore, for each fixed V, a certain number of "trial and errors" steps are required in order to find the right value of E, for which solid and liquid coexist for long time.

Simulations have been performed at a number of points in the pressure range 0-135 GPa. The points on the melting curve obtained from these simulations are displayed in Fig 1, and compared with the experimental results of ZB, and with previously calculated melting curves [4–8]. The solid curve between points has been obtained by interpolating with third order polynomials, with the conditions for the coefficients given by the coordinates and the slopes at the points. The slope of the melting curve is obtained from the Clausius-Clapeyron relation $dT/dp = v_m/s_m$, where v_m and s_m are the volume and the entropy change on melting respectively. For a chosen point on the melting curve (p_m, T_m), v_m is calculated from independent simulations on solid and liquid MgO, with the respective volumes adjusted until the calculated pressures are equal (within ~ 0.5 GPa) to the chosen value p_m. From these simulations it is also possible to obtain s_m, given by $s_m = (e_m + p_m v_m)/T_m$, where $e_m = e_{liq} - e_{sol}$, with e_{liq}, e_{sol} the internal energies in the liquid and the solid simulations respectively. These simulations have been performed on cells containing 64 atoms, for over 40 ps, and spot checked with simulations performed with 216 atoms, which showed essentially no difference in e_m within a statistical error of ~ 10 meV/atom. Pressures calculated with the 64-atom and 216-atom cells differed by less than 0.5 GPa. Results for v_m, s_m and the melting slope are reported in Table II.

As a by-product of the simulations on the liquid state I have also obtained the shear viscosity of the liquid η, calculated using the Green-Kubo relations as described in Ref. [28], this is also reported in Table II. Note that the value of the shear viscosity on the melting curve increases only slightly as a function of pressure.

In order to test the effect of the size of the simulation cell on the melting curve, I have also performed one simulation with 1024 atoms ($4 \times 4 \times 8$ cubic supercell)

at $p \sim 47$ GPa for 11 ps [29]. The melting point (p, T) extracted from this simulation is also reported in Fig. 1, and is essentially indistinguishable from that obtained with the 432-atom cell.

Other systematic sources of errors are associated with the XC functional. In order to test how different approximations for the XC behave, I have used the generalised gradient corrections (GGA)'s known as PW91 [30] and PBE [31], and evaluated GGA - LDA differences in the melting temperature at a number of different pressures. To do so, I have calculated the free energy differences between LDA and the GGA functionals employed, for both solid and liquid, following the techniques described in Ref. [13]. At zero pressure the difference in free energy between LDA and PW91 is 0.1 eV/atom, and the difference between LDA and PBE is essentially the same. When combined with the entropy of melting of ~ 2.2 k_{B}/atom, this difference results in a lowering of the melting temperature of ~ 540 K. This result is in fair agreement with the findings of Tangey and Scandolo [8], who also reported that at zero pressure the GGA melting temperature is lower than the LDA by ~ 450 K. So, similarly to the case of Al [9,17,32], in MgO the GGA underestimates significantly the zero pressure melting temperature. However, this result should not be taken as a general trend of GGA versus LDA, as in Si, for example, the situation is reversed, with the LDA the zero pressure melting temperature being lower than the GGA one [33,34]. At higher pressures the free energy differences between GGA and LDA are greatly reduced, and at 135 GPa the GGA melting temperature is lower than the LDA one by only ~ 100 K.

Finally, I have tested the effect of the choice of the distribution between valence and core electrons in the Mg potential, by evaluating the free energy differences between the MgO system represented with the couple of Mg and O PAW potentials described above and the system in which the Mg PAW potential was chosen to have both $3s^2$ and $2p^6$ in valence. The free energy differences are extremely small, both at zero and at high pressure, and result in corrections to the melting temperature of 26 K and 69 K at 0 and 135 GPa respectively. These corrections have been included in the results reported in Fig. 1

The present results for the melting curve of MgO, based on first principle simulations of direct coexistence of solid and liquid, support the "high" melting curve previously indicated by a number of theoretical approaches based on empirical potentials [4–7], but are at variance with the experimental results of ZB. The agreement between the LDA and GGA predictions for the high pressure melting curve of MgO suggests that the expected systematic error due to the XC functional employed may be small. However, this is not the case in the low pressure region, where the difference between LDA and GGA is of the order of $\sim 18\%$. This relatively large discrepancy points towards the need of going beyond DFT with the current implementations of the XC functionals. We believe that one possible way forward will be the use of quantum Monte Carlo techniques [35].

The predicted high melting curve of MgO has important consequences for our understanding of the Earth's lower mantle and the history of the Earth's formation. The melting temperature of the mantle is constrained between the melting temperatures of the end members Mg(Fe)O-magnesiowüstite and Mg(Fe)SiO$_3$-perovskite, and the eutectic point. The very high melting temperatures of both MgO and MgSiO$_3$ (between 7000 and 8500 K [36]) indicate that the eutectic temperature of the lower mantle is much higher than its current temperature (estimated to be between 2550 and 2750 K) and than the temperature at the top of the core (~ 4000 K). This would suggest that the presence of partial melt of Mg-bearing phase in the ultra-low velocity zone at the bottom of the Earth's mantle is unlikely.

[1] T. S. Duffy, R. J. Hemley, and H.-K. Mao, Phys. Rev. Lett. **74**, 1371 (1995).

[2] Q. Williams and E. J. Garnero, Science **273**, 1528 (1996).

[3] A. Zerr and R. Boehler, Nature, **371**, 506 (1994).

[4] L. Vočadlo and G. D. Price, Phys. Chem. Min., **23**, 42 (1996)

[5] R. E. Cohen and Z. Gong, Phys. Rev. B, **50**, 12301 (1994)

[6] A. B. Belonoshko and L. S. Dubrovinsky, Am. Min. **81**, 303 (1996)

[7] A. Strachan, R. Çağin, and W. A. Goddard III, Phys. Rev. B **63**, 096102 (2001).

[8] P. Tangney and S. Scandolo, unpublished.

[9] D. Alfè, Phys. Rev. B, **68**, 064423 (2003).

[10] T. Ogitsu, F. Schwegler, F. Gygi, G. Galli, Phys. Rev. Lett., **91**, 175502 (2003)

[11] S. A. Bonev, F. Schwegler, T. Ogitsu, G. Galli, Nature **431**, 669 (2004).

[12] J. R. Morris, C. Z. Wang, K. M. Ho, and C. T. Chan, Phys. Rev. B **49**, 3109 (1994).

[13] D. Alfè, G. D. Price, M. J. Gillan, J. Chem. Phys, **116**, 7127 (2002).

[14] A. B. Belonoshko, R. Ahuja, O. Eriksson, and B. Johanson, Phys. Rev. B **61**, 3838 (2000).

[15] J. R. Morris, X. Song, J. Chem. Phys., **116**, 9352 (2002).

[16] A. Aguado, P. A. Madden, Phys. Rev. Lett. **94**, 06850 (2005).

[17] G. A. de Wijs, G. Kresse and M. J. Gillan, Phys. Rev. **57**, 8223 (1998).

[18] W. C. Mackrodt, in *Computer Simulation of Solid* edited by C. R. A. Catlow and W. C. Mackrodt (Springer Verlag, Berlin, 1982), p. 175.

[19] A. De Vita, M. J. Gillan, J. S. Lin, M. C. Payne, and Štich, L. J. Clarke, Phys. Rev. B **46** 12964 (1992).

[20] D. Alfè and M. J. Gillan, to appear in Phys. Rev. B(R)

[21] G. Kresse and J. Furthmüller, Phys. Rev. B, **54**, 111((1996).

[22] D. Alfè, Computer Phys. Commun., **118**, 31 (1999).

[23] P. E. Blöchl, Phys. Rev. B **50**, 17953 (1994).

[24] G. Kresse and D. Joubert, Phys. Rev. B **59**, 1758 (1999.

[25] N. D. Mermin, Phys. Rev. **137**, A1441 (1965).

[26] H. J. Monkhorst and J. D. Pack, Phys. Rev. B **13**, 51: (1976).

[27] Initial velocities are assigned according to a Maxwellian distribution.

[28] D. Alfè and M. J. Gillan, Phys. Rev. Lett., **81**, (1998).

[29] Each step of molecular dynamics took ∼ 6 minutes and 50 seconds respectively for the 1024-atom and 432-atom systems, on 128 processors of an IBM-regatta machine with POWER4+ processors running at a clock speed of 1.7GHz.

[30] Y. Wang and J. Perdew, Phys. Rev. B **44**, 13298 (1991); J. P. Perdew, J. A. Chevary, S. H. Vosko, K. A. Jackson, M. R. Pederson, D. J. Singh and C. Fiolhais, Phys. Rev. B **46**, 6671 (1992).

[31] J. P. Perdew, K. Burke, M. Ernzerhof, Phys. Rev. Lett., **77**, 3865 (1996).

[32] L. Vočadlo and D. Alfè, Phys. Rev. B, **65**, 214105 (2002).

[33] O. Sugino and R. Car, Phys. Rev. Lett. **74**, 1823 (1995).

[34] D. Alfè and M. J. Gillan, Phys. Rev. B, **68**, 205212 (2003).

[35] W. M. C. Foulkes, L. Mitaš, R. J. Needs, and G. Rajagopal, Rev. Mod. Phys. **73**, 33 (2001).

[36] A. Zerr and R. Boehler, Science, **262**, 553 (1993).

[37] B. B. Karki, R. M. Wentzcovitch, S. de Gironcoli, and S. Baroni, Phys. Rev. B **61**, 8793 (2000).
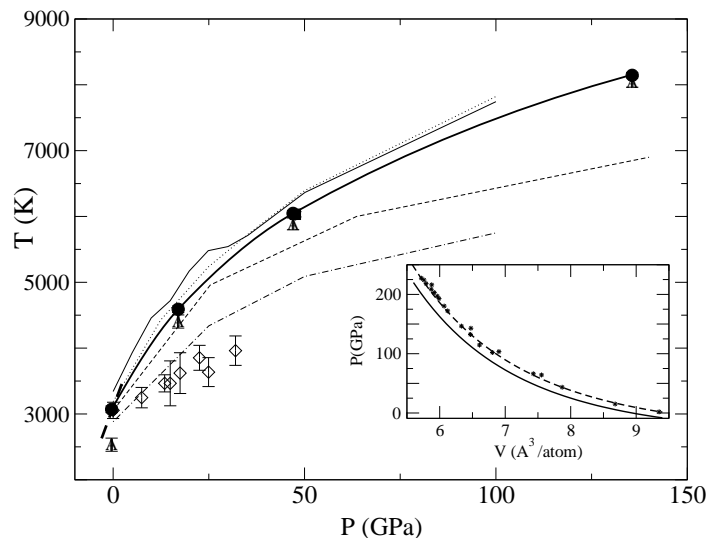
FIG. 1. Melting curve of MgO obtained with present DFT-LDA coexistence simulations performed on 432-atom cells (black dots and heavy solid line), 1024-atom cell (black square), and present DFT-GGA results (triangles), compared with experiments (open diamonds) [3] and theoretically determined curves based on empirical potentials: Belonoshko and Dubrovinski (chained line) [6], Strachan et al. (dashed line) [7], Cohen and Zong (dotted line) [5], Vočadlo and Price (solid line) [4], Tangney and Scandolo (heavy dashed line) [8]. Inset: pressure as function of atomic volume for rock-salt MgO calculated with DFT-LDA (solid line) and DFT-GGA (dashed line), and compared with experiments (stars) [1]. Calculations do not include zero point motion.

	a_0(Å)	B_0(GPa)	$P_{\rm tr}$(B1-B2) (GPa)
Experiments	4.213[a] 4.211[b] 4.212[c] 4.19[d]	160±2[a] 160.2[c] 156[e] 164.6[d]	> 227[f]
DFT-LDA (large core)	4.151(4.180)	180(170)	503
DFT-LDA (small core)	4.165(4.194)	177(167)	505
DFT-GGA (PW91)	4.234(4.263)	158(148)	491

TABLE I. Experimental and calculated lattice parameter a_0 and bulk modulus B_0 of MgO in the NaCl structure (B1), and transition pressure $P_{\rm tr}$(B1-B2) between the NaCl and the CsCl (B2) structures. Values in parenthesis include zero point motion and room temperature effects estimated from Ref. [37]. The calculations labelled "large core" have been performed with the Mg potential with only the $3s^2$ electrons in valence, while those labelled "small core" with the Mg potential with both the $3s^2$ and the $2p^6$ electrons in valence.

p_m (GPa)	$T_m^{\rm LDA}$ (K)	$T_m^{\rm GGA}$ (K)	dT/dp (K/GPa)	v_m (Å^3/atom)	s_m ($k_{\rm B}$/atom)	η (mPa s)
-0.4(2)	3070(50)	2533(100)	102(5)	3.08(5)	2.19(10)	3.0(4)
17.0(2)	4590(50)	4405(100)	62(3)	1.44(5)	1.69(4)	3.8(3)
47.0(2)	6047(40)	5887(90)	33(2)	0.73(3)	1.59(3)	4.5(4)
135.6(2)	8144(40)	8044(80)	16(1)	0.34(2)	1.51(2)	5.0(4)

TABLE II. Calculated melting properties of MgO: pressure p_m, LDA and GGA melting temperatures $T_m^{\rm LDA}$ and $T_m^{\rm GGA}$, slope of the melting curve dT/dp, volume and entropy change on melting v_m and s_m, and shear viscosity of the liquid η at the melting point. All quantities (except $T_m^{\rm GGA}$) have been calculated using DFT-LDA.